Support effects on CO oxidation on metal-supported ultrathin FeO(111) films

Xuefei Weng,[+] Ke Zhang,[+] Qiushi Pan, Yulia Martynova, Shamil Shaikhutdinov,*
Hans-Joachim Freund

Abteilung Chemische Physik, Fritz-Haber-Institut der Max-Planck-Gesellschaft, Faradayweg 4-6, 14195 Berlin, Germany

Abstract: FeO(111) films grown on a Au(111) substrate were studied in the low temperature CO oxidation reaction at near-atmospheric pressure. Enhanced reactivity over the otherwise inert Au(111) surface was only observed if the iron oxide films possessed so-called "weakly bound oxygen" (WBO) species upon oxidation at elevated pressures. The reaction rate measured under O-rich conditions (CO/O_2 = 1/5, totally 60 mbar, He balance) was found to correlate with the total amount of WBO measured in the "oxidized" films by temperature programmed desorption. The initial reaction rate measured as a function of the film coverage showed a maximum at about one monolayer (ML), in contrast to ~ 0.4 ML obtained for the Pt(111)-supported FeO(111) films measured with the same setup. When compared to FeO(111)/Pt(111), WBO species on FeO(111)/Au(111) desorb at a much lower (i.e., by ~ 200 K) temperature, but also in much smaller amounts. Scanning tunneling microscopy studies showed that the FeO(111) layer on Au(111) is fairly stable towards high pressure oxidation in the low coverage regime, but undergoes substantial reconstruction at near-monolayer coverages, thus resulting in poorly-defined structures. Comparison of structure-reactivity relationships observed for Au(111) and Pt(111) supported FeO(111) films revealed the complex role of a metal support on reactivity. While a strong interaction with the Pt(111) surface stabilizes a planar, FeO(111)-derived structure for the active oxide phase, in the case of a more weakly interacting Au(111) surface, the reaction atmosphere induces structural transformations governed by the thermodynamic phase diagram of the iron oxide, albeit it seems crucial to have a dense FeO(111) film as the precursor.

Key words: Ultrathin films; Iron oxides; CO oxidation; Support effects

*Corresponding author: shaikhutdinov@fhi-berlin.mpg.de

[+] These authors contributed equally to this work.

Introduction

Ultrathin oxide films grown on metal substrates receive much attention as advanced materials with superior functional properties in modern technological applications.[1-4] In particular for catalysis, well-ordered oxide films were recognized as suitable models for elucidating the atomic structure and mechanisms of chemical reactions on oxide surfaces and oxide supported metal nanoparticles.[3, 5-14] Recently, ultrathin transition-metal oxide films have been invoked to rationalize the so-called Strong Metal/Support Interaction which often results in an encapsulation of metal particles by a thin oxide overlayer stemming from the support.[15-18] In addition, the systems consisting of oxide nanostructures (primarily, as two-dimensional islands) grown on a metal surface have been studied to address reactions that may occur at the metal/oxide interface in conventional, oxide-supported metal catalysts.[2, 19, 20]

Our recent studies of various metal-supported ultrathin films in CO oxidation revealed an inverse relationship between the reaction rate and the binding energy of the most weakly bound oxygen (WBO) species which was suggested as a good descriptor for CO oxidation on continuous (dense) films.[21] Those WBO species were detected via temperature programmed desorption (TPD) measurements of the films exposed to pure oxygen (typically 10 mbar) at the reaction temperature. Although the precise mechanism of O_2 desorption from such films remains unknown, the desorption temperature can be used as a qualitative measure of the WBO binding energy.

If the oxide film partially covers a metal substrate, CO adsorption on such systems becomes crucial as well. Indeed, the CO oxidation rate on ZnO(0001) films increased considerably at sub-monolayer (sub-ML) coverages when grown on Pt(111), but not on Ag(111).[22, 23] The effect was reasonably explained by a much stronger CO adsorption on Pt(111) as compared to Ag(111) which, in turn, increases the residence time for adsorbed CO to react with WBO supplied by ZnO. Therefore, the CO adsorption energy can be considered as another descriptor for the reaction,

which may even dominate at sub-ML oxide coverages. This has recently been demonstrated for FeO(111) islands deposited on Pt(111).[24] Both experimental and theoretical results provided strong evidence that, in addition to the reaction pathway on the oxide surface as observed on a continuous film, the reaction primarily occurs between CO adsorbing on Pt and WBO species at the island edge. Note that WBO species were only observed at a high chemical potential of oxygen (i.e. elevated oxygen pressures). Once formed, they readily react with CO even under UHV conditions thanks to the strong CO adsorption on the Pt sites available at sub-ML coverages.

Previous studies including density functional theory (DFT) calculations showed that, under reaction conditions, an FeO(111) monolayer film on Pt(111) transforms into an "O-rich" FeO_{2-x} structure which can be described, for simplicity, as an O-Fe-O trilayer, [25] although the precise structure appears to be more complex due to the Moire superstructure caused by the lattice mismatch between the oxide layer and the support. According to our TPD study, [24] the same transformation occurs for FeO(111) films at sub-ML coverages. However, in their studies, Bao and coworkers concluded that the FeO_2–like structures are inert, [26] and the reactivity must be linked to coordinatively unsaturated Fe cations at the edges of pristine FeO(111) islands which dissociate O_2.[27-29] Oxygen ions, which bind both to Pt and Fe, are responsible for the facile CO oxidation.

In attempts to shed more light on the reactivity of metal supported ultrathin films and elucidate the role of a metal support, in this work we address the reactivity of the FeO(111) films on Au(111) and compare the results with those from the previously studied FeO(111)/Pt(111) system. In principle, gold is the most inert noble metal with respect to both CO and O_2, and therefore, one can readily assign the observed reactivity (if any) to the iron oxide phase. In addition, the Au(111) surface has a surface lattice constant and a work function quite different from those of Pt(111). Both parameters may be crucial for the phase stability and oxygen induced phase transformations.

The preparation of an FeO(111) film on Au(111) has first been reported by Matranga and coworkers [30] by oxidation of Fe deposits with molecular O_2. A combined scanning tunneling microscopy (STM) and x-ray photoelectron spectroscopy (XPS) study showed the formation of FeO(111) monolayer islands and a continuous film exhibiting a Moire structure very similar to that previously observed for FeO(111)/Pt(111). Under certain preparation conditions using NO_2 as an oxidizing agent, other iron oxide structures can be formed, which were assigned to Fe_2O_3(0001) [31] and Fe_3O_4(111).[32] Interestingly, ambient pressure XPS studies revealed that a continuous Fe_2O_3 film showed a different response to elevated pressures of CO (0.2 Torr) as compared to nanoparticulate Fe_2O_3.[33] Recently, Fe_2O_3/Au(111) model catalysts have been examined by Yan *et al.* [34] in the CO oxidation reaction at pressures between 4 and 100 Torr and temperatures from 400 to 670 K. The authors observed a maximum rate at 0.4 ML coverage (as determined by Auger electron spectroscopy, AES), suggesting the active cites to be located at the Fe_2O_3/Au(111) perimeter. Yu *et al.* [35] compared the activities of differently prepared iron oxide/Au(111) model catalysts, which were characterized by XPS before and after the reaction in the mixture of 5 Torr CO and 5 Torr O_2 at 575 K. The results showed that neither FeO nor Fe_2O_3 is stable under the reaction conditions used, and both transform into the Fe_3O_4–like phase. Interestingly, the initial reaction rate was found to be the highest on FeO(111)/Au(111) as a starting material.

Results and discussion

As the reactivity studies were carried out in the UHV setup which was not equipped with STM to measure the FeO(111) coverage directly, we first address coverage calibration which is, in fact, not a trivial issue. Film thicknesses estimated from XPS and/or AES measurements using tabulated values for fitting parameters (such as a mean free path of electrons and a cross section) which are commonly derived from experiments performed on few nanometers thick films becomes rather inaccurate in the case of ultrathin, i.e. monolayer films (see, for instance, refs.[36,

37]).

In our previous study of FeO(111) films supported by Pt(111), the oxide coverage in the sub-monolayer range could be determined by CO titration of the bare Pt surface with TPD since FeO(111) does not chemisorb CO.[24] Precise morphology of the islands should not affect the CO uptake results as the DFT calculations showed only small changes of the CO adsorption energy for the Pt sites close to FeO(111) islands as compared to the regular sites. Figure 1a demonstrates that the intensity ratio of the O (at 512 eV) and Pt (at 237 eV) Auger electrons is linearly proportional to the FeO coverage measured by CO uptake. In the case of Au(111) as a substrate, the metal surface could hardly be titrated by CO and other probe molecules. All desorption signals on Au(111) at temperatures above 90 K (only accessible with our setup) are commonly associated with the surface defects. On the other hand, Au and Pt, being neighbors in the Periodic Table, exhibit similar fingerprints in AES (and XPS). A very small kinetic energy difference of Auger electrons in Au and Pt (239 and 237 eV, respectively) implies the same mean free path. Also, the elemental sensitivity of the corresponding Auger line in Au is only ~ 5 % higher than in Pt.[38] Moreover, since the measurements on both systems were carried out with the same spectrometer and the same parameters (e.g. excitation energy, oscillation voltage, acquisition time, etc) all apparatus effects are self-cancelled. Therefore, the FeO(111) coverage on Au(111) can fairly well be determined by measuring the intensity (I) of the O(512 eV) and Au(241 eV) signals taking into account a 5% higher elemental sensitivity of Au as compared to Pt. This finally results in the FeO(111) coverage (θ_{FeO}, in ML) on Au(111) as: $\theta_{FeO} = A \times I(O_{512\,eV})/I(Au_{239\,eV})$, with a scaling factor A = 0.95 (± 0.1).

In addition, Figure 1b shows that the Auger O/Au ratio is linearly proportional to the Auger Fe(653 eV)/Au(241 eV) intensity ratio measured before the oxidation step, thus suggesting that the compositional stoichiometry of the FeO(111) film remains unchanged in this coverage regime. At high coverages the results scatter most likely due to the formation of different iron oxide domains.[30]

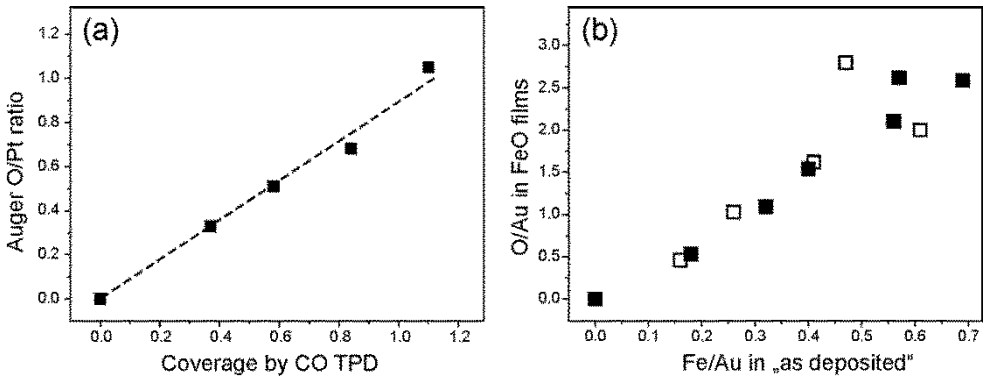

Figure 1. (a) The relationship between the Auger O(512 eV)/Pt(237 eV) signal ratio and film coverage obtained for FeO(111)/Pt(111) films and measured by CO titration. (NB: The sample at 1.1 ML showed no CO uptake and the coverage was determined by extrapolation using the Fe deposition time). (b) The relationship between the Auger Fe(653 eV)/Au(239 eV) signal ratio obtained after Fe deposition on Au(111) and the O(512 eV)/Au(239 eV) signal ratio measured after oxidation step. The opened and filled symbols show data for the samples used for reactivity studies and structural characterization upon high pressure oxygen treatment, respectively (see text).

Furthermore, AES measurements in another chamber, additionally equipped with STM that allowed measuring the FeO(111) coverage directly (see images below), showed a similar linear relationship, although yielding a lower scaling factor A = 0.75 (± 0.15). Note, however, that STM as a local probe technique inspects a relatively lower surface area as compared to the TPD technique that averages over the entire sample surface.

Figure 2a shows typical kinetics of CO_2 production measured in the circulating mixture of 10 mbar of CO and 50 mbar of O_2 (He balance to 1 bar) on the pristine and FeO(111) covered Au(111) surfaces at 480 K. The reaction was performed in excess of oxygen in order to prevent film dewetting that occurred in stoichiometric ($CO:O_2$ = 2:1) and CO-rich conditions on the Pt(111) supported films.[16, 39] As expected, the clean Au(111) surface is, in essence, inert in this reaction. (Some CO_2 production can be attributed to reactions on the sample holder and heating wires). Clearly, the iron oxide overlayer considerably promotes the reaction which, however, slows down in time. Therefore, we focus solely on the initial reaction rate, i.e. measured within the

first 10-15 minutes. The rate strongly depends on the FeO(111) coverage and shows a maximum at about 1 ML (Fig. 2b). Data scatter at high coverages where iron oxide phases other than monolayer FeO(111) can readily be formed [30] (see also Fig. 1b). Such a volcano-type curve has previously been observed in our experiments on FeO(111)/Pt(111).[24] However, the rate was the highest at the sub-monolayer coverage (~0.4 ML), so that the promotional effect could straightforwardly be attributed to the reaction at the oxide/metal perimeter sites. Apparently, for the FeO(111) films on Au(111), the reaction is proportional to the total surface area of the FeO(111) phase. These results suggest that: (i) the reaction primarily occurs on oxide surface rather than at oxide/metal interfacial sites; (ii) at nominal film thickness above 1 ML, other structures start to form which are inactive in this reaction, but dominate at high film thicknesses. Both conclusions well agree with the general picture developed for the Pt(111) supported films as discussed above. Indeed, CO very weakly adsorbs on the Au(111) surface in contrast to Pt(111), and hence the reaction on Au supported islands does not benefit from having the oxide/metal interface. With increasing nominal film thickness above one monolayer, FeO(111) transforms into another phase such as Fe_3O_4(111) which shows no rate enhancement.[16]

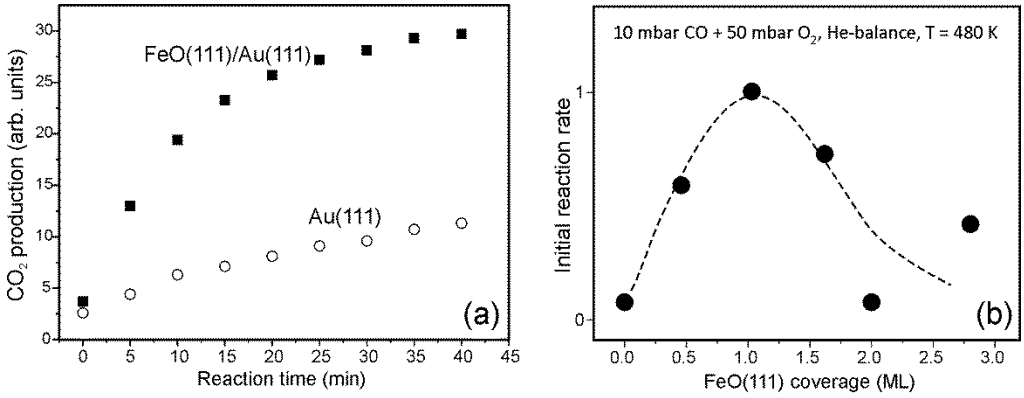

Figure 2. (a) Kinetics of CO_2 production in the circulating mixture of 10 mbar of CO and 50 mbar of O_2 (He balance to 1 bar) on the pristine and FeO(111) covered Au(111) surfaces at 480 K. (b) The initial rate (normalized to the maximum) as a function of the FeO(111) coverage measured by AES.

Since the CO oxidation reaction was performed in the O_2-rich atmosphere, any structural transformations that occur on FeO(111)/Au(111) under reaction conditions are likely governed by oxygen ambient as it was previously shown for FeO(111)/Pt(111).[40] Therefore, in the next set of experiments, we performed structural characterization of the freshly prepared films after exposure to 20 mbar of O_2 at 480 K for 10 min. The samples were cooled down to 350 K before pumping oxygen out.

The low energy electron diffraction (LEED) pattern of an 1 ML FeO(111)/Au(111) film is shown in Fig. 3a. Similarly to FeO(111) films on Pt(111), the "flower"-like diffraction spots are indicative of a Moire-like coincidence structure that was observed by STM ([30], see also below). The FeO(111) integer spots are almost aligned with those of Pt(111). Therefore, in the first approximation, we assume no rotation of the FeO(111) layer with respect to Au(111). Using the surface lattice constant of Au(111) ($\boldsymbol{a}_{Au(111)}$ = 2.88 Å) as an internal reference, we obtained the value 3.14 (±0.04) Å, on average, for the lattice constant of FeO(111). For comparison, the measurements on the Pt(111) supported films performed with the same LEED apparatus yielded 3.06 (±0.03) Å, on average (Fig. 3c). The latter value is considerably lower than 3.11 Å reported by Weiss et al.,[41] who employed a more precise spot profile analysis LEED technique, which is in turn very close to 3.13 Å calculated on the basis of a coincidence structure where eight unit cells of FeO(111) coincide with nine unit cells of Pt(111) ($\boldsymbol{a}_{Pt(111)}$ = 2.78 Å). To some extent, the observed discrepancy on FeO/Pt samples (3.06 Å *vs* 3.11 Å) could be assigned to imperfection of our LEED optics. Using 1.016 (= 3.11/3.06) as the scaling factor, we can recalculate the lattice constant of the FeO(111) layer on Au(111) that yields 3.19 Å. Again, the latter value nicely agrees with 3.20 Å obtained for the situation when nine unit cells of FeO(111) coincide with ten unit cells of Au(111). In fact, such coincidence structure is favored by atomically resolved STM images presented by Khan et al. (see Figs. 8 and 9d in ref. [30]), although the authors themselves preferred the value 3.3 (± 0.3) Å) on the basis of interatomic distances directly measured by STM.

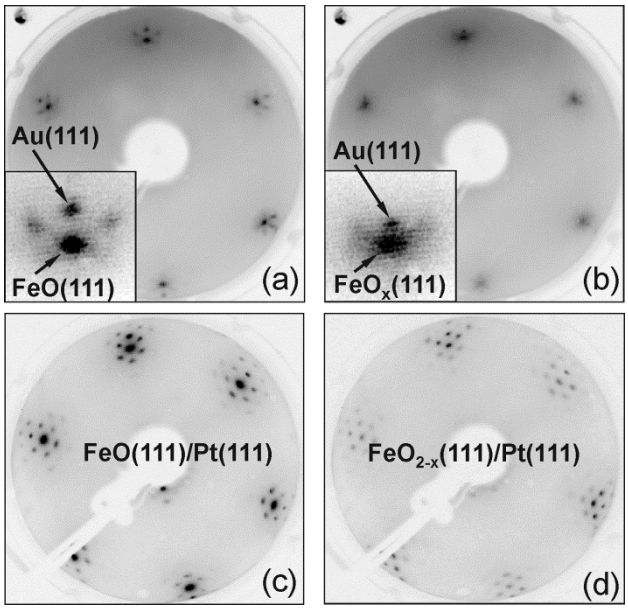

Figure 3. Inverse contrast LEED patterns (at 60 eV) of 1 ML FeO(111) film on Au(111) (a,b) and Pt(111) (c,d) before (a,c) and after (b,d) exposure to 20 mbar of O_2 at 480 K for 10 min. The insets in panels (a,b) zoom in the same figure portion for direct comparison.

Figure 3b displays the LEED pattern of the film upon high-pressure oxygen treatment. The diffraction spots become weaker and broader, thus suggesting certain disordering caused by oxidation. Nonetheless, we found that the film lattice constant is reduced substantially, i.e. from 3.19 to ~3.08 Å. Such a response is very different from that observed on FeO(111)/Pt(111) under the same treatment (see Figs. 3c,d). In the latter case, the film remains highly ordered and no considerable changes in the lattice parameter are detected.

Further AES inspection of the oxygen treated FeO(111)/Au(111) films showed that the Auger O/Fe ratio in the monolayer film increased by ~ 50 % (at most), that is considerably smaller than > 80 % observed for the 0.6 ML and 1 ML FeO/Pt films after exposure to the same conditions.

Finally, the samples were studied by TPD in order to see whether WBO species are formed under high pressure oxygen conditions. Figure 4a shows a series of O_2 (32 amu) desorption spectra recorded on films of different thicknesses as indicated. Note, that the end temperature was limited to ~ 1000 K to avoid a risk of damaging (e.g.

melting) the Au crystal at higher temperatures. A sharp desorption O_2 peak is observed at 635 K which was missing on the "as prepared" FeO(111)/Au(111) surface and on the clean Au(111) surface after the same treatment. Therefore, this signal can straightforwardly be assigned to WBO species which are only formed at elevated oxygen pressures. Interestingly, the total amounts of WBO follow the same volcano-type curve as the reaction rate, both showing a maximum at ~ 1 ML coverage (*cf* Figs. 4b and 2b).

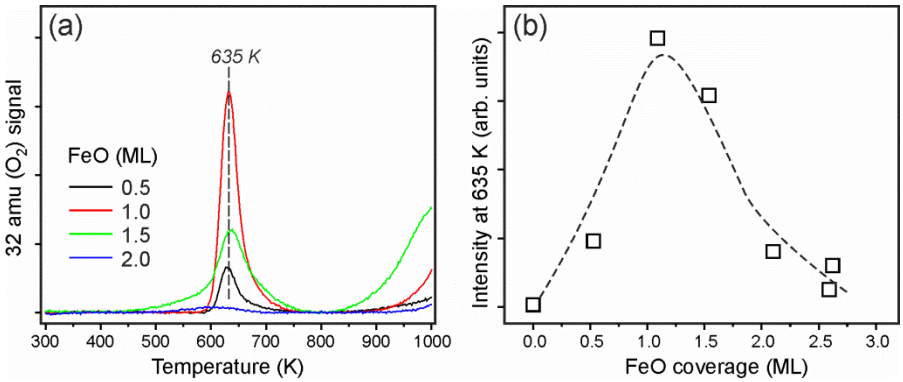

Figure 4. (a) 32 amu (O_2) signal in TPD spectra of FeO(111)/Au(111) films exposed to 20 mbar O_2 at 480 K for 10 min. The heating rate is 3 K/s. (b) The integral intensity of the desorption peak at 635 K plotted as a function of the nominal film thickness.

To shed more light on the structural transformations induced by oxidation at high pressures, we carried out STM studies in another UHV setup. Figure 5a shows large-scale STM image of the "as prepared" film at the ~0.5 ML coverage. As in the previously reported STM study by Khan et al., [30] FeO(111) islands are readily identified by the Moire structure with a ~30 Å periodicity. The islands are surrounded by the clean Au(111) surface showing a "herring-bone" reconstruction (Fig. 5b). The apparent height of the islands is about 0.8 Å (depending on the tunneling conditions, though), which can, therefore, be assigned to a single FeO(111) layer. Note also, that under certain tunneling conditions the island edges look much higher than the interior region, thus indicating very different electronic structure of the step edges. In addition, a few particles about 6 Å in height can also be observed on this surface.

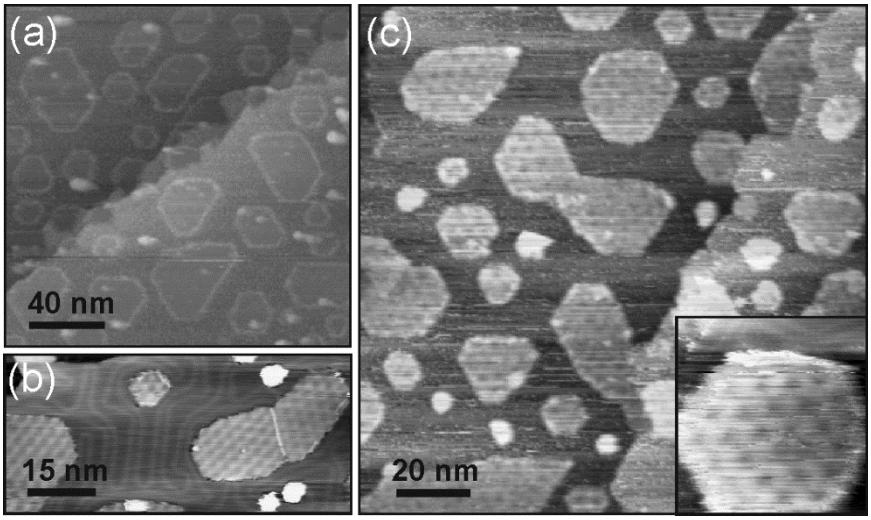

Figure 5. STM images of an 0.5 ML FeO(111) film: (a,b) as-prepared and (c) exposed to 10 mbar O_2 at 470 K for 10 min. The inset shows a close-up image. (Sample bias and tunneling current are: -0.06 V, 0.1 nA (a); -0.7 V, 0.15 nA (b); -1.0 V, 0.14 nA (c); -0.9 V, 0.08 nA (inset)).

An STM image of the film exposed to 10 mbar of O_2 at 470 K is displayed in Fig. 5c. Basically, the film morphology remains the same: The lateral size and shape of oxide islands are not changed, and the "herring bone" Au(111) surface between islands can still be resolved. However, the Moire periodicity on the islands increased from ~30 Å to ~45 Å. This finding well agrees with the LEED results (Fig. 3) showing that the lattice constant considerably decreases upon high-pressure oxidation. Indeed, a shortening of the FeO(111) lattice constant reduces the mismatch with the Au(111) surface and hence increases the periodicity of the coincidence structure, which can be described as $14 \times \boldsymbol{a}_{FeOx} \approx 15 \times \boldsymbol{a}_{Au(111)} = 43.2$ Å, using $\boldsymbol{a}_{FeOx} = 3.08$ Å as suggested by LEED. In addition, the islands height increased from initial 0.8 Å to 1.5 Å, albeit both affected by the tip conditions and tunneling parameters.

Further TPD and AES measurements on this sample revealed a very small O_2 desorption peak at ~ 635 K in TPD spectra, but almost no oxygen enrichment in Auger spectra, in fairly good agreement with the results obtained on low coverage samples in the "first" UHV chamber.

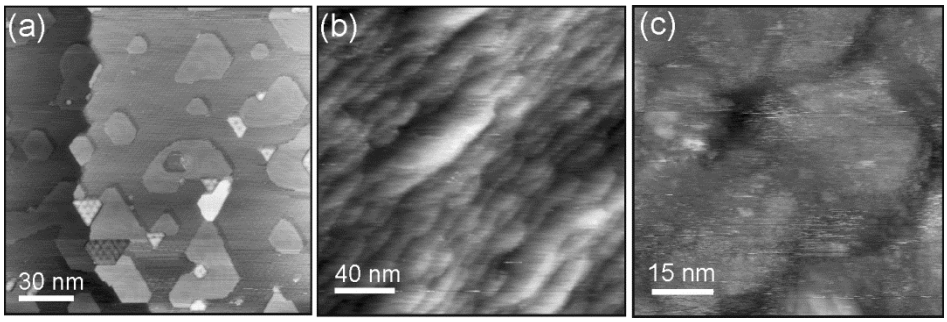

Figure 6. STM images of 1 ML FeO(111)/Au(111) film before (a) and after exposure to 10 mbar O_2 at 470 K (b,c). Tunneling parameters are -1.0 V, 1.2 nA (a,b); -2.1 V, 0.5 nA (c).

Figure 6a shows an STM image of the sample, which was prepared by deposition of enough Fe amount to form a continuous FeO(111) film. The metal and oxide surfaces in the film displayed in Fig. 6a can clearly be distinguished by the "herring-bone" (on Au) and Moire (on FeO) patterns. In contrast to the low coverage regime, Au(111) ad-islands are observed which are surrounded by the FeO(111)/Au(111) surface, thus resulting in the film coverage equivalent to ~ 0.7 ML. To some extent, the formation of Au(111) ad-islands can be attributed to the ~ 4% excess of the Au atoms accommodated in the topmost layer of the reconstructed Au(111) surface, which transforms into the Au(111)-(1×1) structure underneath the FeO(111) layer. In addition, at near-monolayer coverages, some iron is involved in the formation of thicker iron oxide islands also seen in Fig. 6a.

Subsequent oxidation in 10 mbar O_2 at 470 K results in substantial surface reconstruction as shown in Figs. 6(b,c), which is again in contrast to the low coverage regime. The terraces now expose such a rough surface that oxide and metal phases can hardly be differentiated. Nonetheless, this sample showed an amount of WBO a factor of 2 higher than on the 0.5 ML sample, still by an order of magnitude smaller than measured under the same conditions over Pt(111)-supported films. Therefore, the results obtained in two different experimental setups well agree with each other.

In order to rationalize the promotional effect of FeO(111) on reactivity of Au(111) in CO oxidation at near realistic pressure and temperature conditions, let us summarize the key experimental findings as follows:

(1) The reaction rate vs coverage plot shows a volcano-type curve with a maximum at ~ 1 ML coverage;
(2) The reaction rate correlates with the integral amount of WBO species formed in pure oxygen ambient at the reaction pressures and temperatures;
(3) When compared to the Pt(111)-supported films, WBO species on FeO(111)/Au(111) desorb at a much lower temperature (635 K vs 850 K) and in amounts by an order of a magnitude smaller (see direct comparison in Fig. S1 in the Supporting Information, SI);
(4) The morphology of the FeO(111)/Au(111) films oxidized at high oxygen pressures depends on the film coverage: At low coverages, the morphology of islands remains basically the same, although the surface lattice constant decreases from 3.2 to 3.08 Å. At close to monolayer coverages, the films undergo massive reconstruction resulting in poorly defined structures.

Following general considerations discussed in the Introduction, result (1) favors the conclusion that the reaction occurs primarily on iron oxide phase rather than at the oxide/metal interface. Finding (2) further validates this conclusion and suggests that the WBO formation and its replenishment in the catalytic cycle is the rate limiting step. Comparison with the FeO(111)/Pt(111) system shows that WBO species on Au(111) supported films must be more active towards CO. Indeed, temperature dependence for the reaction rate measured on (the most active) 1 ML FeO(111)/Au(111) surface at temperatures between 450 and 500 K revealed the Arrhenius plot (see Fig. S2 in SI) corresponding to the apparent activation energy of 58 kJ/mol. This value is much lower than 113 kJ/mol previously reported for 1 ML FeO(111)/Pt(111), although in stoichiometric CO/O_2 mixture. [16]

On FeO(111)/Pt(111), weakly bound oxygen atoms were identified with the topmost O-layer in a “trilayer” O-Fe-O structure only formed at high chemical potential of oxygen. However, for the FeO(111)/Au(111) system, one encounters certain difficulties to invoke such transformations as the total amounts of WBO

measured by TPD is very low. Also a comparative STM study of the FeO(111) islands before and after high pressure exposure (Fig. 5) does not provide compelling evidence for the formation of a trilayer structure clearly observed on FeO(111)/Pt(111).[18] Instead, the smooth and wave-like long-range periodic surface structure of FeO(111) is maintained. However, there is a certain effect of high pressure oxygen treatment on FeO(111) islands, ultimately causing changes in the surface lattice parameter and island height. On the one hand, such a "thickening" would be consistent with the formation of additional O-layer in the structure. On the other hand, the amount of WBO measured by TPD is equivalent to about 8 additional oxygen atoms that have to be distributed in the entire Moire supercell, which in turn consists of ~ 80 FeO(111) unit cells. In principle, a shortening of the surface lattice constant could readily increase the surface rumpling [42] and hence the apparent height.

Nonetheless, the most active, i.e. close to a monolayer, film substantially reconstructs under the reaction conditions resulting in a structure which is difficult to assign to a particular iron oxide phase (Fig. 6), which, however, possesses the highest amounts of WBO. Taking into account the arguments presented above for the sub-ML films, it seems plausible that the iron oxide phase on Au(111) that becomes active in the CO oxidation reaction, is not represented by a planar, slightly O-rich FeO_{1+x} (111)-derived structure, but yet ill-defined nanoparticulate iron oxide, which has weakly bound oxygen in the structure.

The reaction induced film transformations observed here agree well with the XPS results of Yu et al.[35] who showed that FeO(111) is unstable and transforms into the Fe_3O_4–like phase under applied reaction conditions (although quite different from those used in our work). On the basis of DFT calculations of various iron oxides/metal interfaces, the authors came to the conclusion that Fe_3O_4 is the only active iron oxide phase as it allows O_2 dissociation on active Fe^{2+} sites, available at the particle edge, and subsequent facile reaction with CO. The role of Au in this reaction is to adsorb CO and to provide moderate binding to dissociated O_2, that is similar to the

mechanism first put forward by Sun et al. for the case of FeO(111) layer supported on Pt(111).[28]

While performing reactions at elevated pressures, one has to take precautions with respect to the traces of water in the feedstock. Indeed, recent ambient pressure XPS studies of FeO(111)/Pt(111) provided evidence for the formation of considerable amounts of hydroxyl species even in pure O_2 in the mbar range, [43] in agreement with previous results showing the formation of an FeO(OH)-like film upon water exposure.[44] The dissociation of H_2O resulting in hydroxyl groups at Au(111)-supported FeO(111) island edges was also observed by STM and XPS at water pressures ranging from 3×10^{-8} to 0.1 Torr. [45] Although lattice oxygen in bilayer FeO(111) on Pt(111) does not participate in CO oxidation, CO_2 can readily be formed by CO reacting with such hydroxyl groups as shown by isotopic labelling experiments by Huang and co-workers.[46]

In principle, unsupported nanoparticulate iron oxides are known as good CO oxidation catalysts. For example, a high activity and a low activation energy (~ 70 kJ/mol, compare to 60 kJ/mol in our work) was reported for 3 nm in average size Fe_2O_3 nanoparticles in CO oxidation under O_2 rich conditions at ~ 570 K.[47] Zheng et al. [48] found that quasi-cubic Fe_2O_3 nanoparticles, mainly exposing (110) facets, are even more active, likely due to a higher density of the surface Fe atoms than on the conventionally prepared nanoparticles.

Conclusions

FeO(111) films grown on a Au(111) substrate showed a promotional effect on the reactivity of the otherwise inert Au(111) surface in the low temperature CO oxidation reaction. The reactivity was only observed if the prepared iron oxide films show weakly bound oxygen species upon oxidation at elevated pressures. The reaction rate measured under O-rich conditions (CO/O_2 = 1/10) was found to correlate with the total amount of WBO measured in the “oxidized” film. The initial reaction rate measured as a function of the film coverage showed a maximum at

about 1 ML, in contrast to ~ 0.4 ML obtained for the Pt(111)-supported FeO(111) films measured with the same setup. When compared to FeO(111)/Pt(111), WBO species on FeO(111)/Au(111) desorb at a much lower (i.e., by ~ 200 K) temperature, but also in much smaller amounts. STM studies showed that the FeO(111) layer on Au(111) is fairly stable towards high pressure oxidation in the low coverage regime, but undergoes substantial reconstruction at near-monolayer coverages, thus resulting in poorly-defined structures.

Comparison of structure-reactivity relationships observed for Au(111) and Pt(111) supported FeO(111) films revealed the complex role of a metal support on the reaction. While a strong interaction with the Pt(111) surface stabilizes a planar, FeO(111)-derived structure for the active oxide phase, in the case of a more weakly interacting Au(111) surface, the reaction atmosphere induces structural transformations governed by the thermodynamic phase diagram of the iron oxide, albeit it seems crucial to have a dense FeO(111) film as the precursor. Furthermore, the CO oxidation reaction on the Pt(111) supported films may benefit from the strong CO adsorption on Pt in proximity to the oxygen providing FeO_{2-x} phase, whereas such a mechanism is hardly possible for the Au(111) support due to a very weak CO adsorption.

The results also show that using the “inert” metal support does not solely imply that the reaction occurs only on oxide phase. In fact, the inert support may dramatically affect the reaction through structural transformations, otherwise impossible for the more strongly interacting oxide/metal systems.

Experimental Section

The experiments were performed in two UHV chambers (base pressures ~2×10^{-10} mbar). The first chamber is equipped with LEED, AES (both from Specs), and differentially pumped quadrupole mass-spectrometer (QMS, from Hiden) used for TPD experiments. The Au(111) single crystal (from MaTeck) was spot-welded to the two Ta wires for resistive heating and cooling by filling the manipulator rod with

liquid nitrogen. The sample temperature was measured by a K-type thermocouple inserted into a small hole in the edge of the crystal. The chamber houses a gold plated high-pressure (HP) cell (~ 30 ml) for performing reactivity studies at near atmospheric pressures using a gas chromatograph (GC, from Agilent). For reaction tests, the reaction mixture consisting of 10 mbar CO and 50 mbar O_2, balanced by He to 1 bar, was introduced into the HP cell at room temperature and circulated using a membrane pump for ca 20 min to rich constant flow conditions. Then the sample was heated to the reaction temperature with a rate of 1 K/s. After the reaction, the sample was cooled down to 300 K while pumping the HP cell out down to 10^{-6} mbar before transferring into the main chamber for the post-characterization.

The second chamber is equipped with LEED/AES (Specs), QMS (Hiden) and STM (Omicron). The Au(111) crystal was mounted on the Omicron sample holder and could be heated by electron bombardment from the backside of the crystal. The temperature was measured by a K-type thermocouple at the edge of the crystal. For high pressure treatments, the sample was transferred into the HP cell (base pressure 10^{-8} mbar) separated by a gate valve from the main chamber. The heating in the HP cell was achieved by illuminating the sample with a halogen lamp through the quartz window.

In both chambers, the Au(111) surface was cleaned by cycles of Ar^+ ion sputtering and annealing in UHV at 700 K. Residual carbon was removed by oxidation at 700 K in 10^{-6} mbar O_2. The surface cleanness was checked by AES and LEED (STM) prior to the film growth.

The preparation of an FeO(111) film on Au(111) followed the one reported by Khan et al. [30] Iron was vapor-deposited from a Fe rod (99.99%, Goodfellow) using an e-beam assisted evaporator (Omicron EMT3) at 300 K and then oxidized at 323 K in 3×10^{-7} mbar O_2 for 8 min. The sample was annealed in UHV at 700 K for 10 min.

Acknowledgments

The authors acknowledge Cluster of Excellence UNICAT administered by TU Berlin and Fonds der Chemischen Industrie for financial support.

References

1. Pacchioni, G., *Two-Dimensional Oxides: Multifunctional Materials for Advanced Technologies.* Chemistry - A European Journal, 2012. **18**(33): p. 10144-10158.
2. Netzer, F.P., F. Allegretti, and S. Surnev, *Low-dimensional oxide nanostructures on metals: Hybrid systems with novel properties.* Journal of Vacuum Science & Technology B: Microelectronics and Nanometer Structures, 2010. **28**(1): p. 1-16.
3. Giordano, L. and G. Pacchioni, *Oxide Films at the Nanoscale: New Structures, New Functions, and New Materials.* Accounts of Chemical Research, 2011. **44**(11): p. 1244-1252.
4. Freund, H.-J. and G. Pacchioni, *Oxide ultra-thin films on metals: new materials for the design of supported metal catalysts.* Chemical Society Reviews, 2008. **37**(10): p. 2224-2242.
5. Kuhlenbeck, H., S. Shaikhutdinov, and H.-J. Freund, *Well-Ordered Transition Metal Oxide Layers in Model Catalysis - A Series of Case Studies.* Chemical Reviews, 2013. **113**(6): p. 3986-4034.
6. Weiss, W. and W. Ranke, *Surface chemistry and catalysis on well-defined epitaxial iron-oxide layers.* Progress in Surface Science, 2002. **70**(1-3): p. 1-151.
7. Chambers, S.A., *Epitaxial growth and properties of thin film oxides.* Surface Science Reports, 2000. **39**(5): p. 105-180.
8. Nilius, N., *Properties of oxide thin films and their adsorption behavior studied by scanning tunneling microscopy and conductance spectroscopy.* Surface Science Reports, 2009. **64**(12): p. 595-659.
9. Libuda, J. and H.J. Freund, *Molecular beam experiments on model catalysts.* Surface Science Reports, 2005. **57**(7-8): p. 157-298.
10. Henry, C.R., *Surface studies of supported model catalysts.* Surface Science Reports, 1998. **31**(7-8): p. 231-325.
11. Bäumer, M. and H.-J. Freund, *Metal deposits on well-ordered oxide films.* Progress in Surface Science, 1999. **61**(7-8): p. 127-198.
12. Rainer, D.R. and D.W. Goodman, *Metal clusters on ultrathin oxide films: model catalysts for surface science studies.* Journal of Molecular Catalysis A: Chemical, 1998. **131**(1-3): p. 259-283.
13. Franchy, R., *Growth of thin, crystalline oxide, nitride and oxynitride films on metal and metal alloy surfaces.* Surface Science Reports, 2000. **38**(6-8): p. 195-294.
14. Freund, H.-J., *Adsorption of Gases on Complex Solid Surfaces.* Angewandte Chemie International Edition in English, 1997. **36**(5): p. 452-475.
15. Shaikhutdinov, S. and H.-J. Freund, *Ultrathin Oxide Films on Metal Supports: Structure-Reactivity Relations.* Annual Review of Physical Chemistry, 2012.

63(1): p. 619-633.

16. Sun, Y.N., et al., *Monolayer iron oxide film on platinum promotes low temperature CO oxidation.* Journal of Catalysis, 2009. **266**(2): p. 359-368.
17. Qin, Z.H., et al., *Encapsulation of Pt Nanoparticles as a Result of Strong Metal -Support Interaction with Fe3O4(111).* The Journal of Physical Chemistry C, 2008. **112**(27): p. 10209-10213.
18. Sun, Y.-N., et al., *The Interplay between Structure and CO Oxidation Catalysis on Metal-Supported Ultrathin Oxide Films.* Angewandte Chemie-International Edition, 2010. **49**(26): p. 4418-4421.
19. Hayek, K., et al., *Surface reactions on inverse model catalysts: CO adsorption and CO hydrogenation on vanadia- and ceria-modified surfaces of rhodium and palladium.* Topics in Catalysis, 2000. **14**(1-4): p. 25-33.
20. Rodriguez, J.A., et al., *Inverse Oxide/Metal Catalysts in Fundamental Studies and Practical Applications: A Perspective of Recent Developments.* The Journal of Physical Chemistry Letters, 2016. **7**(13): p. 2627-2639.
21. Martynova, Y., S. Shaikhutdinov, and H.-J. Freund, *CO Oxidation on Metal-Supported Ultrathin Oxide Films: What Makes Them Active?* Chemcatchem, 2013. **5**(8): p. 2162-2166.
22. Martynova, Y., et al., *CO oxidation over ZnO films on Pt(111) at near-atmospheric pressures.* Journal of Catalysis, 2013. **301**(0): p. 227-232.
23. Pan, Q., et al., *Reactivity of Ultra-Thin ZnO Films Supported by Ag(111) and Cu(111): A Comparison to ZnO/Pt(111).* Catalysis Letters, 2014. **144**(4): p. 648-655.
24. Pan, Q., et al., *Enhanced CO Oxidation on the Oxide/Metal Interface: From Ultra-High Vacuum to Near-Atmospheric Pressures.* ChemCatChem, 2015. **7**(17): p. 2620-2627.
25. Sun, Y.N., et al., *The interplay between structure and CO oxidation catalysis on metal-supported ultrathin oxide films.* Angew Chem Int Ed Engl, 2010. **49**(26): p. 4418-21.
26. Fu, Q., et al., *Reversible structural transformation of FeOx nanostructures on Pt under cycling redox conditions and its effect on oxidation catalysis.* Physical Chemistry Chemical Physics, 2013. **15**(35): p. 14708-14714.
27. Fu, Q., F. Yang, and X. Bao, *Interface-Confined Oxide Nanostructures for Catalytic Oxidation Reactions.* Accounts of Chemical Research, 2013. **46**(8): p. 1692-1701.
28. Sun, D., et al., *Theoretical Study of the Role of a Metal - Cation Ensemble at the Oxide - Metal Boundary on CO Oxidation.* The Journal of Physical Chemistry C, 2012. **116**(13): p. 7491-7498.
29. Fu, Q., et al., *Interface-Confined Ferrous Centers for Catalytic Oxidation.* Science, 2010. **328**(5982): p. 1141-1144.
30. Khan, N.A. and C. Matranga, *Nucleation and growth of Fe and FeO nanoparticles and films on Au(1 1 1).* Surface Science, 2008. **602**(4): p. 932-942.
31. Deng, X. and C. Matranga, *Selective growth of Fe2O3 nanoparticles and islands on Au(111).* Journal of Physical Chemistry C, 2009. **113**(25): p. 11104-11109.

32. Deng, X., J. Lee, and C. Matranga, *Preparation and characterization of Fe3O4(1 1 1) nanoparticles and thin films on Au(1 1 1).* Surface Science, 2010. **604**(7-8): p. 627-632.
33. Deng, X., et al., *Reactivity Differences of Nanocrystals and Continuous Films of α-Fe2O3 on Au(111) Studied with In Situ X-ray Photoelectron Spectroscopy.* The Journal of Physical Chemistry C, 2010. **114**(51): p. 22619-22623.
34. Yan, T., et al., *CO oxidation on inverse Fe2O3/Au(111) model catalysts.* Journal of Catalysis, 2012. **294**(0): p. 216-222.
35. Yu, L., et al., *CO Oxidation on Gold-Supported Iron Oxides: New Insights into Strong Oxide–Metal Interactions.* The Journal of Physical Chemistry C, 2015. **119**(29): p. 16614-16622.
36. Hofmann, S., *Auger- and X-Ray Photoelectron Spectroscopy in Materials Science*. Springer Series in Surface Science, ed. L.H. Ertl G., Mills D. 2013, Heidelberg: Springer-Verlag Berlin. 510.
37. Seah, M.P., et al., *Critical review of the current status of thickness measurements for ultrathin SiO2 on Si Part V: Results of a CCQM pilot study.* Surface and Interface Analysis, 2004. **36**(9): p. 1269-1303.
38. Davis, L.E., et al., *Handbook of Auger Electron Spectroscopy*. 1977: Perkin Elmer Corporation, Physical Electronics.
39. Sun, Y.-N., et al., *When an Encapsulating Oxide Layer Promotes Reaction on Noble Metals: Dewetting and In situ Formation of an "Inverted" FeO x /Pt Catalyst.* Catalysis Letters, 2008. **126**(1-2): p. 31-35.
40. Giordano, L., et al., *Oxygen-Induced Transformations of an FeO(111) Film on Pt(111): A Combined DFT and STM Study.* The Journal of Physical Chemistry C, 2010. **114**(49): p. 21504-21509.
41. Ritter, M., W. Ranke, and W. Weiss, *Growth and structure of ultrathin FeO films on Pt(111) studied by STM and LEED.* Physical Review B, 1998. **57**(12): p. 7240-7251.
42. Goniakowski, J. and C. Noguera, *Polarization and rumpling in oxide monolayers deposited on metallic substrates.* Physical Review B, 2009. **79**(15): p. 155433.
43. Johansson, N., et al., *Oxidation of Ultrathin FeO(111) Grown on Pt(111): Spectroscopic Evidence for Hydroxylation.* Topics in Catalysis, 2016. **59**(5): p. 506-515.
44. Ringleb, F., et al., *Interaction of water with FeO(111)/Pt(111): Environmental effects and influence of oxygen.* Journal of Physical Chemistry C, 2011. **115**(39): p. 19328-19335.
45. Deng, X., et al., *In Situ Observation of Water Dissociation with Lattice Incorporation at FeO Particle Edges Using Scanning Tunneling Microscopy and X-ray Photoelectron Spectroscopy.* Langmuir, 2011. **27**(6): p. 2146-2149.
46. Jin, Y., et al., *Water-Activated Lattice Oxygen in FeO(111) Islands for Low-Temperature Oxidation of CO at Pt–FeO Interface.* The Journal of Physical Chemistry C, 2016. **120**(18): p. 9845-9851.
47. Li, P., et al., *The removal of carbon monoxide by iron oxide nanoparticles.* Applied Catalysis B: Environmental, 2003. **43**(2): p. 151-162.
48. Zheng, Y., et al., *Quasicubic α-Fe2O3 Nanoparticles with Excellent Catalytic*

Performance. The Journal of Physical Chemistry B, 2006. **110**(7): p. 3093-3097.